Collagen-Hyaluronic Acid Scaffolds for Adipose Tissue Engineering

N. Davidenko[1,*], J.J. Campbell[2], E.S. Thian[1, 3], C.J. Watson[2] and R.E. Cameron[1]

[1]Department of Materials Science and Metallurgy

University of Cambridge, Pembroke Street

Cambridge, CB2 3QZ, UK

[2]Department of Pathology

University of Cambridge, Tennis Court Road

Cambridge, CB2 1QP, UK

[3]Department of Mechanical Engineering

National University of Singapore, 9 Engineering Drive 1

Singapore 117 576, Singapore

*Corresponding Author.

Email: nd313@cam.ac.uk Tel: +44 1223 334560. Fax: +44 1223 334567

Abstract

Three-dimensional (3D) *in vitro* models of the mammary gland require a scaffold matrix that supports the development of adipose stroma within a robust freely permeable matrix. 3D porous collagen-hyaluronic acid (HA: 7.5 and 15%) scaffolds were produced by controlled freeze-drying technique and cross-linking with 1-ethyl-3-(3-dimethylaminopropyl)-carbodiimide hydrochloride. All scaffolds displayed uniform, interconnected pore structure (total porosity ~ 85%). Physical and chemical analysis showed no signs of collagen denaturation during the formation process. The values of thermal characteristics indicated that cross-linking occurred and that its efficiency was enhanced by the presence of HA. Although the cross-linking reduced the swelling of the strut material in

water, the collagen-HA matrix as a whole tended to swell more and show higher dissolution resistance than pure collagen samples. The compressive modulus and elastic collapse stress were higher for collagen-HA composites. All the scaffolds were shown to support the proliferation and differentiation 3T3-L1 preadipocytes while collagen-HA samples maintained a significantly increased proportion of cycling cells (Ki-67+). Furthermore, collagen-HA composites displayed significantly raised Adipsin gene expression with adipogenic culture supplementation for 8 days versus control conditions. These results indicate that collagen-HA scaffolds may offer robust, freely permeable 3D matrices that enhance mammary stromal tissue development *in vitro.*

Keywords: Collagen; crosslinking; freeze-drying; hyaluronic acid; scaffolds, adipose tissue engineering

1. Introduction

The mammary gland comprises a complex branched epithelial network invested within an adipocyte-rich stroma termed a fat-pad. Uniquely, the majority of mammary gland development is post-natal, where the rudimentary organ penetrates the underlying pre-developed fat-pad under hormonal control, however the influence of the stroma in guiding the formation of this structure has been well documented [1,2]. Accurate 3-dimensional (3D) models of the mammary gland should encourage stromal tissue development as a basis for further epithelial coculture studies. A great deal of research has been carried out with the hope of obtaining an effective means of achieving adipose tissue formation *in-vitro* [3,4]. The most widely-used approach involves locating the relevant cells in a physical 3D scaffold under ‘controlled’ culture conditions, so facilitating cell attachment, proliferation, differentiation and, finally, formation of a tissue structure of suitable shape and size.

To date, the majority of *in vitro* mammary cell and tissue culture investigations utilize reconstituted basement membrane gels (Matrigel™) or pure collagen gels. While useful, native whole tissue preparations such as Matrigel are undefined in composition and exhibit batch variation [5]. Moreover they cannot be tuned to the specific requirements of an *in vitro* model system. Alternatively, pure collagen gels, whilst defined, exhibit cell-mediated matrix contraction [6], varying mechanical properties throughout long-term culture and limiting oxygen and nutrient transport to cells within [7]. Furthermore, gel-based systems are random with regard to cellular distribution and limit direct cell-contact, an important component of coculture signaling mechanisms [8,9]. Currently, there is a great need for more defined *in vitro* mammary gland models that may increase our understanding of basic biological processes, aid drug discovery and minimize intensive animal use with *in vivo* studies. Properly *in-vitro* engineered tissues may offer an excellent possibility of carrying out detailed and continuous control and monitoring of cellular responses, with the further advantage of "humanising" the system by using human cells instead of animal model, which would be more appropriate for drug screening and cancer studies [10,11]. Towards our goal of producing a novel tissue engineered mammary gland, we have developed a naturally derived scaffold with controlled architecture and robust mechanical characteristics that encourages adipose tissue development.

In order to successfully create an artificial 3-dimensional structure capable of supporting *in vitro* tissue formation, several key attributes have to be taken into account. It should be highly porous with an interconnected architecture [12-14]; predictable and controllable material degradability, and should have biocompatibility with the seeded cells to enhance cellular activity [15-17]. It should also possess an adequate mechanical stiffness [18-20] to withstand stress incurred during cell culturing. Furthermore, the formation of a new tissue in the 3D matrix structure is highly influenced by the chemical composition of the

bio-scaffold [21]. ollagen, being a major protein of the natural extracellular matrix (ECM), has been commonly used in the form of a gel for adipose tissue engineering [22-25] in spite of limitations principally related to cell-mediated contraction.

HA, a naturally occurring unsulfated glycosaminoglycan distributed in the ECM of soft tissues [26] has been implicated in diverse biological processes such as angiogenesis and migration [27,28] as well as the proliferation and differentiation of progenitor cells [29]. Recent studies have demonstrated the utility of HA-based scaffolds in enhancing adipose tissue development *in vivo* [30,31] and *in vitro* [32,33].

The combination of collagen and HA has displayed advantages over the use of either material alone for tissue engineering applications [34-40]. For example, the incorporation of HA to the collagen matrix has shown positive effects in stimulating chondrocyte and fibroblast expression *in-vitro* [34-36]. In addition to direct biological effects, the incorporation of HA should enhance the strength of the collagen-based gels, thus inhibiting the cell induced contraction. The properties of scaffolds made from collagen and HA combinations are explored in the current paper.

Freeze-drying, also known as lyophilization, is commonly employed to produce water-soluble polymer scaffolds such as collagen [12, 41-43]. In this technique, a suspension of the water-soluble polymer is frozen, thereby forming an interpenetrating network of ice crystals. Next, these ice crystals are removed by reducing the chamber pressure to induce sublimation, thus leading to the formation of a porous scaffold. A controlled freezing process during production normally leads to uniform nucleation and growth of ice crystals and hence the formation of a homogeneous pore structure. With a well-defined pore structure, improved biomechanical properties of the scaffold can be achieved [43, 44].

To enhance the structural stability of collagen-based sponges various chemical and/or physical cross-linkers are frequently introduced in the production process [43, 45, 46]. EDC

(in the presence of N-hydroxysuccinimide, NHS) and glutaraldehyde (GTA) are two of the most commonly used chemical agents which work in a distinctly different manner. EDC forms “zero length” crosslinks, whereas GTA crosslinks take the form of long polymer chains. This means that EDC is limited to crosslinking collagen/HA molecules that are directly adjacent to each other (1nm) whereas GTA can crosslink molecules that are rather more separated. However, the incorporation of GTA into scaffolds can have implications for biocompatibility. EDC, on the other hand, is known as a non-toxic and biocompatible cross-linker because it generates peptide-like bonds. Cross-linking EDC, in the presence of NHS, produces substituted urea as a by-product which can be easily eliminated by washing.

In this study, the reaction with water soluble EDC in the presence of NHS was selected. This crosslinking process is governed by certain complex mechanisms [45,46]. On the basis of many results, Pieper *et al.* [47] have concluded that EDC/NHS can be utilised for attaching glycosaminoglycans (GAGs), such as: dermatan sulphate, heparin and chondroitin sulphates, to collagen. These findings suggest that similar reactions may occur between collagen and HA because of the similarity of the HA chemical structure to the other GAGs .

In the current study, therefore, the formation of defined collagen-HA scaffolds containing various amounts of HA and with uniform pore structure, and hence good mechanical properties, suitable for tissue engineering purposes, using a freeze-drying technique and non-toxic and biocompatible cross-linking system, is investigated. Some relevant structural, physico-chemical, mechanical and biological characteristics of such scaffolds are defined.

2. Materials and methods

2.1. Collagen and Collagen-Hyaluronic Acid Scaffold preparation

The highly porous scaffolds were produced from a collagen-HA suspension using a freeze-drying technique. Firstly, the suspension of 1%-wt. of different component compositions were prepared from an insoluble, type I microfibrillar collagen derived from bovine Achilles tendon (Sigma-Aldrich Co. Ltd., UK) and HA derived from bovine vitreous humor (Sigma-Aldrich Co. Ltd., UK) in 0.05 M acetic acid solution (Sigma-Aldrich Co. Ltd., UK), where the resultant pH value was adjusted to below 2.0 with 1 M hydrochloric acid (VWR International Ltd., UK). Each suspension was then blended at 20,000 rpm using an overhead homogenizer for 30 min at 40C. After mixing, the suspension was centrifuged at 2500 rpm for 5 min using a bench-top centrifuge to remove air bubbles formed during the blending. Two different HA weight percentages were produced: 7.5 and 15 wt-% (collagen-7.5HA and collagen 15HA, respectively), in addition to suspensions were made with pure collagen.

The prepared collagen and collagen-HA suspensions were then frozen in 316L stainless steel plates at a controlled rate (0.9°C min^{-1}) to -30°C and held for 90 min, using a computer-controlled freeze-dryer. The frozen suspensions were subsequently sublimed at 0°C for 20 h under a vacuum of less than 100 mTorr.

2.2. Scaffold Crosslinking

Lyophilized collagen and collagen-HA scaffolds were crosslinked with a water-soluble carbodiimide. Scaffolds were immersed in 95 % ethanol solution containing 33mM of 1-ethyl-3-(3-dimethylaminopropyl)- carbodiimide hydrochloride (EDC, Sigma-Aldrich Co. Ltd., UK) and 6mM of N-hydroxysuccinimide (NHS, Sigma-Aldrich Co. Ltd., UK) for 4 h at 25°C. After the crosslinking process, the scaffolds were washed thoroughly in distilled water (5 min x 5) and were subsequently re-frozen and re-lyophilized using the previous freeze-

drying cycle. Disc samples of diameter 10 mm were then cut from sheets of scaffolds using a punch.

2.3. Scaffold morphology

X-ray microtomography (Skyscan 1072 Micro-CT (μCT) system), with a 28 kV/ 164 μA X-ray source (using 0-360^{o} range of rotation angle with a step size of 0.45^{o} and 3.1 sec of exposure time per step) and provided with 12-bit cooled CCD camera, was employed to obtain a general view of the interior microstructure of the scaffolds. Cross-sections were generated using a full cone beam Feldkamp reconstruction algorithm.

Analysis of the scaffold pore structure was carried out on a scanning electron microscopy (SEM) (JEOL 5800). Samples were sputter-coated with a layer of platinum for observation at 10kV at various levels of magnification.

2.4. Physicochemical Analysis of Scaffolds

X-ray study

Changes in the structural composition of the scaffolds were identified using a Philips PW3020 X-ray Diffractometer (XRD) with CuK_{α} radiation operating at 40 kV and 40 mA. θ-2θ scans were performed and data were collected over a 2θ range of 5-35°, with a step size of 0.05° and a dwell time of 10 s.

FTIR analysis

A BRUKER Tensor 27 Fourier Transform Infrared Spectrometer (FTIR), utilizing the attenuated total reflectance technique, was used to analyze the molecular structure of the scaffolds. The spectra were collected over a range of 1000-4000 cm^{-1} to monitor any changes in the amide groups. A resolution of 4 cm^{-1} was used, and the samples were scanned 16 times to increase the signal-to-noise ratio.

Porosity

The porosity level of the scaffolds was determined using a computer-controlled Quantachrome Poremaster 33 Mercury Intrusion Porosimeter (MIP by applying various levels of pressure to a sample immersed in mercury (Hg). The pressure required to intrude mercury into the sample pores is inversely proportional to the size of the pores. To perform an analysis a known quantity of each scaffold (between 0.0036g and 0.0038g) was loaded into a penetrometer. The penetrometer was sealed and placed in a low pressure chamber, where the sample was evacuated for 5 min at 0.05 torr to remove air and moisture, and then automatically backfilled with mercury (filling pressure 6.6kPa). Subsequently the penetrometer was moved to a high-pressure chamber and subjected to pressure in steps from 0.69kPa to 206Mpa. After completing this process Hg was extruded from the sample pores by stepwise pressure reduction and the extruded volume of Hg corresponding to each step was recorded. The porosity level (%) was then automatically calculated from intrusion data using software provided by this equipment.

2.5. Differential scanning calorimetry (DSC) and thermogravimetric analysis (TG)

The thermal stability of the collagen–HA matrix was assessed with DSC Q2000 and TGA Q 500 analyzers scanning from 0 to 450°C. The samples were weighed and placed into aluminium pans. The pans were heated at a constant rate of 10°C min^{-1} in a nitrogen atmosphere. In the case of DSC testing, an empty aluminium pan was used as reference. The sample mass was in the range of 1-3 mg. All samples were run in duplicate. The denaturation temperatures were measured at the mid-point of the transition peaks and the temperatures at the start of the process were measured at the onset of the peak. From the TG and DSC curves obtained by means of the Universal Analysis software, the following parameters, which describe the thermal behaviour of these scaffolds, were calculated: temperatures of thermal denaturation (Td), maximum temperature of each decomposition stage (T_1-T_3); percentage of the corresponding mass loss (Δm %), and total mass loss at 450^{o}C in nitrogen (Δm_{total}).

2.6. Water Uptake of Scaffolds

Dried samples were weighed prior to the swelling study (W_d). Next, the samples were immersed in 5 ml distilled water at 37°C for different periods of time up to 7 days. At each time point, they were removed from the distilled water and two different measurements of their capacity to retain water were made.

The first measurement was aimed at assessing the ability of the scaffold structure as a whole (the material itself together with the pore system) to absorb water. For this, at each time point, the samples were removed from water, shaken gently, and then weighed without dripping (W_{ws}).

The second measurement was carried out after pressing and "drying" the same soaked samples between sheets of filter paper to remove the water retained in its porous structure (W_{wm}). In this way the swelling ability of scaffold material itself was determined.

The percentage of water uptake, in both cases, was calculated as shown:

Water uptake (%) = $[(W_w – W_d) / W_d] \times 100$

Where W_w represents W_{ws} or W_{wm}.

2.7. Dissolution of Scaffolds

Dried samples were weighed prior to the dissolution study (W_b). The samples were then immersed in 5 ml distilled water at 37°C in a humid atmosphere for various periods of time, up to 7 days. At each time point, they were removed from the distilled water, dried for 48h (under reduced pressure to constant weight) and weighed (W_a). The percentage weight loss was calculated as shown:

Weight loss (%) = $[(W_b – W_a) / W_b] \times 100$

The pH value of the distilled water after each time interval was measured using a pH meter. Each sample was measured in triplicate.

2.8. Mechanical Analysis of Scaffolds

Compressive stress-stain analysis of the scaffolds was performed using a Mechanical Tester. Scaffolds were immersed in distilled water at 37°C in a humid atmosphere for 24 h before testing. A cell load of 5 N and a crosshead speed of 5 mm min^{-1} were used. Mechanical characteristics which describe stress–strain behaviour, namely: the linear elastic (Young's) modulus (E*), the elastic collapse stress and strain (σ^*_{el}, ε^*_{el}), and the slopes of the collapse plateau ($\Delta\sigma/\Delta\varepsilon$) were determined from each curve for all scaffolds tested. E* was obtained via linear regression of the initial linear region of the stress–strain curve; $\Delta\sigma/\Delta\varepsilon$ was calculated via linear regression of the linear region following the ''knee'' corresponding to the strut bending–buckling transition; σ^*_{el} and ε^*_{el} were determined from the intersection of the E* and $\Delta\sigma/\Delta\varepsilon$ regression curves (see Fig.10b and explanation of stress-strain profiles in Results and Discussion part). Five replica tests were made for each scaffold.

2.9. Preadipocyte cell culture within 3D scaffolds

A murine preadipocyte (3T3-L1) cell line (a generous gift from Prof. Kenneth Siddle, University of Cambridge) was grown to passage 5 in Dulbecco's modified eagles medium (DMEM) + 10% (vol/vol) newborn calf serum (Invitrogen, UK). Pure collagen and collagen mixed HA scaffolds were sterilized by UV exposure and rinsed thrice in both distilled H_2O and PBS before 5 scaffolds of each type were bathed in a 10ml suspension of 3T3-L1 cells at a density of $1x10^6$ cells/ml in a 50mL Falcon tube. Scaffolds were compressed onto the wall of each tube using a sterile pipette in order to remove air bubbles and encourage cell penetration throughout the scaffold. Each scaffold/cell suspension was then gently agitated on a rocker plate for 4 hours at 37°C to encourage further cell penetration. Cell seeded scaffolds were then removed to an incubator for 3 days until confluence judged by live-cell fluorescent visualization with 5μM Calcein-AM (Invitrogen, UK). Terminal differentiation of 3T3-L1

preadipocytes was induced by incubation for 48 h within DMEM, 10% fetal calf serum (FCS, Hyclone, Thermofisher), 1μM dexamethasone, 0.5mM 3-isobutyl-1-methylxanthine and 0.01mg/ml insulin (all Sigma-Aldrich Co. Ltd., UK) followed by a further 6 days incubation in DMEM, 10% FCS and insulin. Adipogenic control specimens were incubated for 8 days in DMEM + FCS.

2.10. Oil-Red O and Immunohistochemical staining

Following 8 days adipogenic induction, cell-seeded scaffolds were fixed in 4% paraformaldehyde/PBS embedded and frozen within O.C.T and cryosectioned at 10μm. Lipid was stained with Oil-Red O and counter stained with haematoxylin using routine methods. For immunohistochemistry, sections were blocked at room temperature for 1hr with 10% normal goat serum (Sigma-Aldrich Co. Ltd., UK), incubated with an anti-Ki67 primary antibody (Abcam, UK) overnight at 4°C and detected with an Alexafluor 488 conjugated secondary antibody (Invitrogen, UK). Nuclei were stained with Hoerscht 33258. Proliferation rate was measured by scoring Ki-67 positive nuclei in a x200 field of view.

2.11. Gene expression analysis

Cell-seeded scaffolds exposed to adipogenic or control culture conditions were snap frozen in liquid nitrogen. Total RNA was extracted using Trizol reagent (Invitrogen) and an RNeasy mini kit (Qiagen) following the manufacturers instructions. cDNA was reverse transcribed from 1μg of total RNA using 0.5U/μl reverse transcriptase (Roche) and random primers (Promega). Adipogenic gene expression was analysed by real-time quantitative PCR (Biorad Icycler Biorad Laboratories Inc, USA) using SYBR green chemistry (Sigma). Sequences for real-time PCR were obtained using the PrimerBank [48] website (http://pga.mgh.harvard.edu/primerbank/) for peroxisome proliferator-activated receptor gamma (PPARγ), Fw: TCGCTGATGCACTGCCTATG, Rv:

GAGAGGTCCACAGAGCTGATT and adipsin, Fw: CATGCTCGGCCCTACATGG, Rv: CACAGAGTCGTCATCCGTCAC. Relative mRNA abundance for each gene of interest was measured against a pooled sample standard and expressed as a ratio of *cyclophillin A* Fwd, CCTTGGGCCGCGTCTCCTT, Rev, CACCCTGGCACATGAATCCTG for each sample.

3. Results and discussion

3.1. Scaffold preparation

It is well known that polymer scaffolds for use in cell culture must be highly porous with large surface/volume ratios to provide sufficient space for cell growth and proliferation [43]. The pore structure determines the matrix permeability for diffusion of nutrients and waste products within the scaffolds and its size must be large enough to allow infiltration of the cells towards the centre of the scaffolds. At the same time, it should be sufficiently small so as to provide adequate ligand density for cellular attachment. Development of highly porous scaffolds by a freeze-drying approach was used in this work due to the advantage of this method in employing only water upon freezing as a porogen. Freeze-drying conditions consisting of a relatively high freezing temperature (-30°C) and a rather slow rate of cooling (less that 1°C min^{-1}) were chosen to achieve the formation of highly connected ice crystals of rather large size (100 or more micrometers). After sublimation of these ice crystals under vacuum at 0°C, sponges with the inner morphology (pore size, shape, distribution, interconnectivity, etc.) that mirror the structure of these ice crystals were obtained.

3.2. Structure Morphology

Fig. 1 shows a series of μCT images taken of sections of various scaffolds formed using the freeze-drying technique. Generally, all scaffolds were highly porous, interconnected, and appeared to be relatively homogenous throughout the bulk of the scaffold. A fairly uniform pore structure characterized by thin collagen and collagen-HA

struts was obtained. However, several zones of larger pore sizes (Fig. 1A, area 1) and of material densification, especially at the edges of the scaffold sheets, were detected (Fig. 1A, area 2).

Scanning electron microscope images (Fig. 2) of the different types of cross-section of all scaffolds showed a continuous structure of irregular but rather uniformly distributed interconnected pores. The pore dimensions estimated from SEM microphotographs by the manual measurement of pore zones with arbitrary shapes were mostly in the range of 100 to 220 μm, and were similar for all scaffold compositions. It was logical to expect that the inner morphology of all scaffolds would be similar given that the same freezing conditions were employed for their production. This in turn suggests that the presence of HA does not alter the characteristics of water dispersion in the collagen-HA mixture and leads to the formation of a similar ice structure during the freezing process.

Heterogeneity in the scaffold microstructures (the presence of large pores, local regions of higher density, etc.) may be partially the result of the relatively high concentration of collagen or collagen-HA suspension (1%-wt) used for scaffold preparation. Difficulties in achieving completely uniform collagen-type sponges from rather highly concentrated suspensions (≥ 1%-wt) were reported in other works [49]. It was also reported that scaffolds obtained from less concentrated suspensions (0.5% -wt) displayed a more uniform pore microstructure but their mechanical properties were fairly poor in comparison with those exhibited by sponges achieved from more concentrated suspensions. Structural non-uniformities within the microstructure could cause some variation in the values of several physico-chemical and mechanical characteristics of these systems, but it is necessary to compromise when selecting experimental conditions so as to achieve desirable resultant properties when considering the practical application of scaffolds.

3.3. Porosity Level and Pore Size

All the samples had almost identical porosity (of about 85 %) (data not shown) regardless of the HA level incorporated into the collagen scaffolds.

3.4. Structural and molecular Compositions

X-ray study

Fig. 3 shows the XRD patterns obtained for various crosslinked scaffolds. All patterns showed no sign of collagen denaturation, with the emergence of a distinct peak centered at $2\theta = 7°$ which is indicative of the position of the characteristic equatorial peak of collagen. Furthermore, a broad peak between $2\theta = 15\text{-}18°$ indicated the position of the characteristic interchain spacing of the collagen triple helix.

FTIR-analysis

The FTIR spectra of all the scaffolds exhibited several features characteristic of the molecular organization (Fig. 4). Peptide bonds give rise to several infrared active vibration modes and there was no significant evidence of change in the spectra with HA addition. The presence of amide I band at 1780 cm^{-1} arose due to the stretching vibration of C=O groups in the peptide groups. In addition, the presence of amide II bands at 1623 and 1535 cm^{-1} arose due to the motion combining both the amide N-H deformation and C-N stretching vibrations. Besides these bands, amide N-H stretching vibration modes could be obtained at both 3290 and 3058 cm^{-1} [50,51]

XRD and FTIR analyses confirmed that no other chemical entities were introduced into the crosslinked scaffolds, during the crosslinking reaction. As such, the ability to custom-make collagen-HA scaffolds with appropriate ratios can be easily controlled by altering the initial ratios of the two starting biopolymers.

3.5 Differential scanning calorimetry and thermogravimetric analysis

Differential scanning calorimetry and thermogravimetric measurements were used in order to detect the temperature of denaturation, Td, of pure collagen and collagen–HA scaffolds and to assess their thermal stability. It is expected, that modification (by crosslinking) in the molecular organization of scaffolds should induce favourable variations in their thermal behaviour. It is worth mentioning that the effect of temperature on the conformational properties of these systems is still not clearly elucidated.

Examples of typical DSC and TG thermograms of cross-linked scaffold matrices are shown in Fig. 5. The profiles show four different endothermic peaks: the first, within the temperature range from 30°C to about 130°C, relates to the temperature of thermal denaturation of the scaffold matrix, and the other three are connected with a complex phenomenon of thermal modification, finally leading to the destruction of materials. Parameters describing the thermal behaviour of these scaffolds, calculated from TG and DSC curves, are displayed in Table 1.

It is known [52], that the temperature of thermal denaturation is related to the transition from the triple helix to a randomly coiled conformation, this taking place in the domains between the crosslinks of collagen macromolecules. The stability of this conformation should depend upon the presence of intra- and inter-molecular hydrogen bonds as well as hydrogen-bound water and, as reported [52,53], is strongly influenced by the water content in the matrix and its degree of crosslinking between chains. The values of Td found in this work were very similar for all scaffolds (Table 1), being slightly shifted to the region of higher temperatures in the case of collagen-15HA samples (from ~ 80°C for collagen and collagen-7.5HA to 86.2°C for collagen-15HA). The comparison of these values with that reported for a non-crosslinked collagen matrix (69.5°C [52]) may indicate that the crosslinking process occurred in all the scaffolds and that its efficiency was enhanced by the presence of HA, with the consequent increase of the thermal stability of samples. The

denaturation parameters obtained for collagen and collagen-HA samples are in the range of data reported in the literature for analogous systems [43, 52, 54]. This thermal transition was accompanied by a gradual mass decrease (~ 10%), as observed in the TG curve (Fig. 5) and in Table 1. The major weight loss at 450°C in nitrogen, 77.7±2.0%, was found for pure collagen scaffold while the HA containing matrices showed a somewhat lower percentage of degradation under the same heating conditions: 74.4% and 73.6% for collagen-7.5HA and collagen-15HA, respectively.

The quite similar values of Td found for all scaffolds suggest that the thermal denaturation depends rather more on the degree of hydration and on the degree of cross-linking of scaffolds than on the presence of HA.

3.6. Water Uptake

Scaffold swelling properties have been shown [35, 43, 55] to significantly influence cell behaviours such as adhesion, growth and differentiation. Water uptake properties indicate the level of cell culture medium which will be absorbed by the scaffold during culturing. The results of water-uptake studies are displayed in Fig. 6 (for soaked samples, including the water in both the material and the pores) and in Fig. 7 (after removing water from the pores using filter paper). Each value was averaged from at least five parallel measurements.

It can be seen that in both cases the majority of the water uptake occurred within the first two hours and seemed to have stabilized after 24 h soaking time. However the values of the percentage of water retention in each test showed an opposite trend with the composition of the scaffold. For scaffolds soaked in water this parameter (indicating the water present in the materials and the pores of the scaffold) increases with the increase of HA content in the scaffold matrix (Fig. 6): 15HA>7.5HA>pure collagen = 8300% > 7600% > 6600% at 7 days, while for the samples “dried” by filter paper (indicating the water present in the strut material

of the scaffold alone) the reverse dependence was found: pure collagen>7.5HA>15HA = 488% > 373% > 298% at 7 days.

Generally, the water uptake ability of scaffolds, as sponge-like matrices, should be controlled principally by two aspects: the hydrophilicity of their materials and the stability of their porous structures in water [38, 39, 56]. The hydrophilicity of collagen-HA scaffold compositions is simultaneously influenced by the following antagonistic factors: the polarity of the scaffold material and the formation of crosslinks between macromolecular components. The presence of HA in scaffolds is expected to enhance the polarity of the polymer composition, and positively influencing its swelling. At the same time, the addition of HA should contribute to the intermolecular bonding by creation of ion complexes between its carboxylic groups and amino groups of collagen, which should diminish the swelling ability [56]. Furthermore, HA should also form ester-type linkages between its carboxylic groups and amino and/or hydroxyl groups of collagen, in the presence of EDC/NHS cross-linkers, in this way providing covalent attachment of HA to collagen. The decrease of the swelling capacity of the scaffold materials in the presence of HA (Fig. 7) suggests that HA enhances the crosslinking degree of scaffolds and, in spite of its possible positive contribution to the polymers polarity, diminishes hydrophilic property of these systems.

On the other hand, the degree of cross-linking of sponge-like scaffolds, as shown in [38, 57], strongly influences the structural stability of these 3D matrices, and should contribute to better water retention by their porous structure. The results of overall percentage water uptake found for these scaffolds (Fig. 6) are in agreement with this supposition, as matrices with increased content of HA (higher crosslinked density) show higher values of this parameter, despite the fact that the material itself has a lower value of water absorption. Because of the highly porous nature of the scaffold structure (porosity more that 85%), the degree of material swelling does not play a significant role in overall water retention. It was

found that this contribution was also dependent on the scaffold composition and diminished with increase in HA content: 7.4%: 4.9% and 3.6% for collagen, collagen-7.5HA and collagen-15HA, respectively after 7 days? This again confirms the importance of scaffold structural stability, enhanced with the rise of the degree of crosslinking, to achieve good absorbent characteristics. These results are in agreement with those reported by Park *et al* [38] where greater swelling properties were found for crosslinked collagen-HA membranes in comparison to non-cross-linked samples. In spite of the fact that, in general, the swelling or hydrophilic property of materials is decreased as the degree of cross-linking is increased [39], the authors explained the observed phenomenon by assuming that the stability of a sponge-like porous network played a more important role in water retention than hydrophilicity of the material itself. They stated that the cross-linked matrices could maintain their structural integrity in water, so keeping their swelling ability, whilst poorly cross-linked sponges collapsed and partially lost their porous structure when dipped in distilled water.

The structural integrity of scaffolds after water-uptake studies was confirmed by analysing SEM images of samples which were swollen in water at 37°C for 10 days and then re-frozen and re-lyophilized using the previous freeze-drying cycle. From these images (Fig. 8) it can be seen that there is no visible change in the morphology of the scaffolds, which indicates that the structural integrity of all scaffold compositions remain unaltered in the aqueous environment over this period of time. This suggests that even though there is likely to be some pore closure in water in the scaffolds with lower HA levels, the overall structural integrity remains good after 10 days.

3.6. Dissolution

The resistance to dissolution of various crosslinked scaffolds is shown in Fig. 9. All samples appeared to remain intact throughout the dissolution study. The pure collagen matrices lost more weight during their period in water (19.2% in 7 days), and the majority of

mass loss (16.8%) occurred within 24 h , probably due to migration of unbound or weakly crosslinked collagen molecules from the scaffold structure. The collagen-HA scaffolds exhibited a slower dissolution rate (11.4% and 13.3% in 7 days for collagen-7.5HA and collagen-15HA, respectively), which could be a sign of the higher crosslinked degree of these biopolymer composites. The slightly greater percentage weight loss for scaffold richer in HA might result from the dissolution and removal of free HA molecules [35, 38, 39], a phenomenon which should increase with increasing HA content. The increase of the scaffold resistance to dissolution in the presence of HA could indicate the improvement in the overall structural integrity of the scaffolds which should delay their hydrolytic dissolution. This effect is important in the control of mechanical strength of the scaffold during tissue regeneration. The results obtained are in agreement with those reported for water-uptake studies (Fig. 6) where the higher swelling percentage of collagen-HA scaffolds as a whole was explained by the contribution of HA to the intermolecular bonding with collagen, leading to enhancement of the structural stability of the scaffold matrix in water.

It is appropriate to point out that these results reveal the resistance to dissolution of the scaffolds under study in an aqueous media lacking in enzymatic activity. However it is known that hyaluronic acid can be degraded hydrolytically by a family of enzymes called hyaluronidases (HAse, EC 3.2.1.35) and that in the presence of these enzymes the internal *N*-acetyl-hexosamine glucosidic linkages in the hyaluronan structure may be cleaved to liberate oligosaccharides (residues of glucuronic acid and *N*-acetylglucosamine). These degradation products could migrate from the scaffold to the dissolution media, so altering the apparent rate of their dissolution. As HA based scaffolds developed in this work could be used for a number of different applications, including those *in vitro* and *in vivo*, the assessment of their dissolution rates in the presence of enzymes would be of interest and of practical use to determine scaffold stability in specific culture media. On the other hand, in this particular

study we believe that the presence of serum in our culture media may act as a blocking agent to any inherent enzymatic activity. The inhibitory effect of serum on hyaluronidase activity has been noted in a number of clinical conditions. In addition hyaluronidase has not been directly implicated in mammary gland development so we restricted the dissolution experiments solely to assessing scaffold behavior in distilled water.

The hydrolytic degradation of free or weakly bound collagen/HA molecules extracted from scaffolds caused, in all cases, a very similar drop in pH values (from ~5.78 to ~3.6), which mainly occurred within 24 h of soaking. After this time the pH of all aqueous solutions remained almost unchanged.

3.7. Mechanical Properties

It has already been demonstrated that scaffold microstructure and stiffness affects the bioactivity of these systems [57]. The migration speed of cells on two-dimensional (2D) substrates depends on the stiffness of the substrate. Characterization of the stiffness of the tissue-engineered scaffold would allow the effect of this parameter on cell activity in a more realistic 3D environment to be determined.

Different kinds of mechanical testing are used to determine the effect of various parameters on the stiffness of scaffolds. Many studies carry out tensile testing to determine, for example, the influence of crosslinking on the mechanical properties of collagen-type matrices. However, it was shown [43, 49] that the compressive properties such as Young's modulus and the compressive strength, are of greater interest when studying the impact of substrate properties on cellular activity because cells, through their action, tend to bend and buckle individual struts within the scaffold [58]. So in this work compressive testing in the wet stage of all scaffolds prepared was carried out to determine the influence of scaffold composition on the compressive modulus and other important mechanical characteristics of these matrices.

Typical profiles of compressive stress–strain curves obtained for hydrated collagen and collagen-HA scaffolds are shown in Fig. 10. To assess the scaffold's behaviour under successive compressions the same sample specimen were repeatedly testing at least three times. Strain-stress curves corresponding to this testing (Fig. 10a) revealed no significant changes in their profiles up to a stain of 0.5 (the second and third testing curves overlay each other). The profiles are characterized by three distinct regimes: a linear elastic regime, a collapse plateau and a densification zone (Fig. 10) which are typically observed in deformation (under compression) of low-density, open-cell foams with an interconnected network of struts [49, 59]. As the microstructure of the studied scaffolds resembles that of low-density, open-cell foams, the analogous deformation mechanisms in compression for both systems are expected. Models describing strain-stress behaviour of these foams [59] can be used to explain the compressive performance of these scaffolds. According to these models, each regime of the stress–strain curve provide information about different structural changes occurring in the 3D network: the linear elastic regime is controlled by struts bending; a collapse plateau zone reflects struts buckling and the beginning of pore collapse when a densification regime responds to the completion of pore collapse throughout the material [59].

Mechanical characteristics which describe stress–strain performance were calculated from each curve as explained in the Materials section. According to the cellular solid theory, almost all of these characteristics depend on the relative density ($\rho^*/\rho s$) of the foam, so that for all scaffolds studied this parameter was calculated from the dry density of each freeze-dried sample (ρ^*) and the known dry density of solid collagen ($\rho s = 1.3$ g cm^{-3}) [46] and HA ($\rho s = 1.0$ g cm^{-3}) [60]. As expected, no significant variation in $\rho^*/\rho s$ (see Table 2) was found among the scaffolds. This result could be expected since all scaffolds were produced from the same suspension concentration (1%-wt) under identical experimental conditions. The effect

of scaffold composition on all mechanical properties calculated in the wet stage is reported in Table 2. The mechanical performance of these systems in terms of compressive modulus (E*), collapse plateau modulus (□□□□□□and elastic collapse stress (σ^*_{el}) are also shown in Figures 11 and 12. It can be seen that collagen-HA scaffolds exhibited higher values of these parameters compared to the pure collagen matrix and the increase in HA content enhanced the values of E* and σ^*_{el} (Fig. 11 and 12). In accordance with the cellular solid theory the Young's modulus (E*) and elastic plateau stress σ^*_{el} (also called the compressive strength) depend on the foam relative density ($\rho^*/\rho s$), the Young's modulus of the solid from which the foam is made (Es), and a constant related to the cell geometry. As $\rho^*/\rho s$ and cell geometry are the same for all samples studied, it is logical to assume that the presence of HA contributes to the enhancement of Es, by increasing the crosslinked density of the scaffold struts. Therefore, the inclusion of HA in the scaffold composition increases the stiffness of these systems by the formation of additional crosslinks between collagen and HA molecules, in this way contributing to the resistance of the struts to bending under compression. These results are in agreement with those of Harley *et al* [49] where a significant effect of cross-linking efficiency on E* and σ^*_{el} was observed for collagen-GAG sponges. It was also reported [45, 47] that the presence of GAG contributes to the formation of extra cross-links via EDC in collagen-type scaffolds.

The values of collapse plateau modulus were also higher for collagen-HA scaffolds (Table 2, Fig. 11) but this parameter did not increase steadily with rise in HA content. This may possibly suggest that the strut buckling ($\Delta\sigma/\Delta\varepsilon$), which is expected to be the primary mechanism for pore collapse, is not equally affected as strut bending (E*) by stiffness of scaffold material.

On the other hand, elastic collapse stain, ε^*_e, was found to be constant for all scaffolds (Table 2). These results are compatible with those obtained for collagen-GAG scaffolds [46] where no effect of crosslink density on the ε^*_{el} – a criterion expected to be characteristic of the scaffold microstructure and not stiffness- was detected. In addition, these results can be reasonably explained by the cellular solid theory, which states that the elastic collapse stain is independent of strut stiffness, Es, and, as a consequence, should not be affected by the differences in scaffold cross-linking density.

The error in values of mechanical properties could be the result of some heterogeneity in scaffold microstructures which, as have been shown [61, 62], has a significant effect on mechanical properties and could contribute to the variation in the measured values.

3.8. Three-dimensional preadipocyte cell culture and adipogenesis

Collagen and collagen-HA scaffolds supported both cell proliferation and adipogenic differentiation. Cells not exposed to the adipogenic cocktail (control conditions) maintained a higher proportion of cycling cells than those exposed to the adipogenic cocktail in all scaffold types, by measure of Ki-67 positive nuclei. In addition cells within collagen-15HA scaffolds displayed an increased percentage of cycling cells versus those in pure collagen scaffolds under control conditions, whilst similarly under differentiating conditions cell proliferation in these scaffolds was elevated over both pure collagen and collagen-7.5HA ($p<0.05$) (Fig 13 A). An end-stage analysis of adipogenesis was confirmed by oil-red-O staining of lipid containing vesicles in differentiated 3T3-L1 cells in both pure collagen and HA mixed scaffolds (Fig 13 B,C. Lipid (l) indicated by arrows). It was noted that lipid was more confined to the edges of HA mixed scaffolds than pure collagen (data not shown). Gene expression of adipsin, an enzyme involved in lipid metabolism predominantly located in mature adipocytes [63] was significantly elevated in HA-mixed collagen scaffolds ($p<0.05$, student T-test) subjected to 8 days of adipogenic culture against control culture conditions

(Fig 13 D). In a similar manner PPARγ, a principle transcription factor of adipogenesis [64] was also elevated in HA mixed scaffolds compared to control samples, although unlike adipsin expression, PPARγ exhibits a transient expression profile throughout an adipogenic time course [65] meaning that any significant modulation in the expression of this gene may have been missed. A concominant role for proliferation with adipogenesis has been described, where re-entry into the cell cycle with several rounds of mitotic division following confluence are a preliminary feature of the adipocyte terminal differentiation programme [66]. Therefore, by supporting cell proliferation, the inclusion of HA to collagen scaffolds may aid adipogenesis both by hastening cell-contacted growth arrest prior to adipogenic conversion, a noted requirement for adipocyte conversion [65], and support the early stages of the differentiation programme itself. Although hyaluronic acid based scaffolds have been shown to be supportive of adipocyte culture *in vivo* [31] and *in vitro* [32,33], this is the first time that varying HA concentration within a 3D substrate has been shown to influence both the differentiation and proliferation characteristics of 3T3-L1 preadipocytes. Further work will more comprehensively investigate the performance of these scaffolds *in vivo* and *in vitro,* specifically as 3D substrates for mammary fat-pad tissue engineering, supporting the development of both stromal and epithelial mammary tissues.

4. Conclusions

Highly porous collagen-HA scaffolds containing different amounts of HA, with a uniform interconnected pore structure of diameter 150-200 μm, were produced in this study by a controlled freeze-drying technique. Crosslinking of collagen-HA scaffolds using an EDS/NHS system proves to be an easy, effective and contaminant-free technique. The characteristic of the scaffolds obtained is that of a fairly uniform, uni-axial, interconnecting

porous network, which should assist cell ingrowths, rapid vascularisation, and transfer of oxygen, nutrients and waste products [15-17].

XRD and FTIR analyses indicated that no other chemical entities were introduced into the crosslinked scaffolds, except for the formation of stable amide linkages. As such, the ability to custom-make collagen-HA scaffolds with appropriate ratios, can be easily controlled by altering the initial ratios of the two starting biopolymers.

Swelling tests showed that the water uptake of the scaffold as a whole was higher for collagen-HA samples and increased with HA content. However, the scaffold material alone, (once the water in the pores was discounted) showed the opposite trend. The pure collagen sample also lost more weight during the period of dissolution study, and the majority of mass loss occurred within 24 h. The collagen-HA scaffolds exhibited a slower dissolution rate in distilled water due to the higher degree of cross-linking in the biopolymer composite. These phenomena could be due to the enhancement of bonding between collagen and HA during crosslinking and improvement in the overall structural integrity of the scaffold, thereby delaying the process of dissolution. This effect is important in the control of mechanical strength of the scaffold during cell culture and tissue regeneration.

The increase in HA content gives rise to an increase in the stiffness of these systems which enhanced the values of the mechanical characteristics by the formation of additional crosslinks between collagen and HA molecules, and thus contributed to the resistance of the struts to bending under compression.

Collagen HA mixed scaffolds increased the proportion of proliferative 3T3-L1 preadipocytes in addition to enhancing adipogenic conversion with adipogenic media supplementation.

These results indicate that freeze-dried collagen mixed HA scaffolds may offer robust, freely permeable three-dimensional matrices that enhance mammary stromal tissue

development *in vitro.* In summary, collagen-HA can be considered as a valuable biomaterial for constructing tissue-specific scaffolds for adipose tissue engineering applications.

Acknowledgements

The authors acknowledge support from the Biotechnology and Biological Sciences Research Council, United Kingdom and the NC3Rs initiative.

References

1. Sakakura T, Nishizuka Y, Dawe CJ. Mesenchyme-dependent morphogenesis and epithelium-specific cytodifferentiation in mouse mammary-gland. Science 1976;194(4272):1439-1441.

2. Naylor M, Ormandy C. Mouse strain-specific patterns of mammary epithelial ductal side branching are elicited by stromal factors. Dev Dyn 2002;225(1):100-105.

3. Beahm E, Walton R, Patrick Jr CW. Progress in adipose tissue construct development. Clin Plast Surg 2003;30:547-558.

4. Patrick Jr CW. Breast tissue engineering. Ann Review Biomed Eng 2004;6: 109-130.

5. Soofi LJA, Liliensiek SJ, Nealey PF,Murphy CJ. The elastic modulus of MatrigelTM as determined by atomic force microscopy. J Struct Biol 2009;167:216-219.

6. Gentleman E. NEA, Livesay GA, Dee KC. Collagen composite biomaterials resist contraction while allowing development of adipocytic soft tissue in vitro. Tissue Eng 2006;12(6):1639-1649.

7. Zhu YK, Umino T, Liu XD, Wang HJ, Romberger DJ, Spurzem JR, Rennard SI. Contraction of fibroblast-containing collagen gels: initial collagen concentration regulates the degree of contraction and cell survival. In Vitro Cell Dev-An 2001;37:10-16.

8. Shimonishi M, Sato J, Takahashi N, Komatsu M. Expression of type IV collagen and laminin at the interface between epithelial cells and fibroblasts from human periodontal ligament. Eur J Oral Sci 2005;113(1):34.

9. Che Z, Jung T, Choi J, Yoon D, Jeong H, Lee E, et al. Collagen-based co-culture for invasive study on cancer cells-fibroblasts interaction. Biochemical and biophysical research communications, 2006. p. 268-275.

10. Phillips JB. Tissue engineered approaches to modelling the nervous system. Keynote lecture at “Tissue Engineering: a new dimension to animal replacement”, NC3Rs&BBSRS, 1-2April, London, UK, 2009.

11. Brown RA, Phillips JB. Cell responses to biomimetic protein scaffolds used in tissue repair and engineering. Int Rev Cytol 2007;262:75-150.

12. O’Brien FJ, Harley BA, Yannas IV, Gibson LJ. The effect of pore size on cell adhesion in collagen–gag scaffolds. Biomaterials 2005;26:433–41.

13. Zeltinger J, Sherwood JK, Graham DA, Mueller R, Griffith LG. Effect of pore size and void fraction on cellular adhesion, proliferation, and matrix deposition. Tissue Eng 2001;7:557–72.

14. Wake MC, Patrick Jr CW, Mikos AG. Pore morphology effects on the fibrovascular tissue growth in porous polymer substrates. Cell Transplant 1994;3:339–43.

15. Cao Y, Croll TI, Lee JG, Tuch BE, Cooper-White JJ. Scaffolds, stem cells, and tissue engineering: a potent combination. Aust J Chem 2005;58:691.

16. Hutmacher DW. Scaffold design and fabrication technology for engineering tissues - state of the art and future perspectives. J Biomr Sci-Polym E 2001;12:107-124.

17. Ma PX. Scaffolds for tissue fabrication. Mater Today 2004;7(5):30-40.

18. Peyton SR, Putnam AJ. Extracellular matrix rigidity governs smooth muscle cell motility in a biphasic fashion. J Cell Physiol 2005;204:198–209.

19. Grinnell F, Ho CH, Tamariz E, Lee DJ, Skuta G. Dendritic fibroblasts in three-dimensional collagen matrices. Mol Biol Cell 2003;14:384–95.

20. Yeung T et al. Effects of substrate stiffness on cell morphology, cytoskeletal structure, and adhesion. Cell Motil Cytoskel 2005;60:24–34.

21. Chapekar MS. Tissue Engineering: Challenges and Opportunities. J Biomed Mater Res 2000;53:617-620.

22. Lee CH, Singla A, Lee Y. Biomedical applications of collagen. Int J Pharm 2001;221:1-22.

23. Nimni ME, Cheung D, Strates B, Kodama M, Sheikh K. Chemically modified collagen: a natural biomaterial for tissue replacement. J Biomed Mater Res 1987;21:741-771.

24. Hilliou F, Pairault J, Dominice J, Redziniak G. Growth and differentiation of 3T3-F442A preadipocytes in three-dimensional gels of native collagen. Exp Cell Res 1988;177:372-381.

25. Huss FR, Kratz G. Mammary epithelial cell and adipocyte co-culture in a 3-D matrix: the first step towards tissue-engineered human breast tissue. Cells Tissues Organs 2001;169:361-367.

26. Brekke JH, Thacker K. In: Hyaluronan as a Biomaterial (S. Guelcher, J.O. Hollinger, Eds.) An Introduction to Biomaterials, CRC Press, Boca Raton: Florida, 2005. p. 219-240.

27. West D, Kumar S. The effect of hyaluronate and its oligosaccharides on endothelial cell proliferation and monolayer integrity. Exp Cell Res 1989;183(1):179-196.

28. Banerjee S, Toole B. Hyaluronan-binding protein in endothelial cell morphogenesis. J Cell Biol 1992;119(3):643.

29. Gerecht S, Burdick J, Ferreira L, Townsend S, Langer R, Vunjak-Novakovic G. Hyaluronic acid hydrogel for controlled self-renewal and differentiation of human embryonic stem cells. Proc Nat Acad Sci 2007;104(27):11298.

30. Hemmrich K, von Heimburg D, Rendchen R, Di Bartolo C, Milella E, Pallua N. Implantation of preadipocyte-loaded hyaluronic acid-based scaffolds into nude mice to evaluate potential for soft tissue engineering. Biomaterials 2005; 26:7025-7037.

31. Flynn L, Prestwich GD, Semple JL, Woodhouse KA. Adipose tissue engineeringin vivowith adipose-derived stem cells on naturally derived scaffolds. J Biomed Mater Res 2009; 89A(4): 929-941.

32. Flynn L, Prestwich G, Semple J, Woodhouse K. Adipose tissue engineering with naturally derived scaffolds and adipose-derived stem cells. Biomaterials 2007;28(26):3834-3842.

33. Halbleib M, Skurk T, de Luca C, von Heimburg D, Hauner H. Tissue engineering of white adipose tissue using hyaluronic acid-based scaffolds. I: in vitro differentiation of human adipocyte precursor cells on scaffolds. Biomaterials 2003; 24:3125-3132.

34. Huang-Lee LLH, Nimmi M. Crosslinked CNBr-activated hyaluronan-collagen matrices: Effects on fibroblast contraction. Matrix Biol 1994;14:147-157.

35. Park SN, Lee HJ, Lee KH, Suh H. Biological characterization of EDC-crosslinked collagen-hyaluronic acid matrix in dermal tissue restoration. Biomaterials 2003;24:1631-1641.

36. Tang S, Spector M. Incorporation of hyaluronic acid into collagen scaffolds for the control of chondrocyte-mediated contraction and chondrogenesis. Biomed Mater 2007;2:135-141.

37. Kim TG, Chung HJ, Park TG. Macroporous and nanofibrous hyaluronic acid/collagen hybrid scaffold fabricated by concurrent electrospinning and deposition/leaching of salt particles. Acta Biomater 2008;doi:10.1016/j.actbio.2008.06.008.

38. Park SN, Park JC, Kim HO, Song MJ, Suh H. Characterization of porous collagen/hyaluronic acid scaffold modified by 1-ethyl-3-(3-dimethylaminopropyl) carbodiimide cross-linking. Biomaterials 2002;23:1205-1212.

39. Rehakova M, Bakos D, Vizarova K, Soldan M, Jurickova M. Properties of collagen and hyaluronic acid composite materials and their modification by chemical crosslinking. J Biomed Mater Res 1996;30:369-372.

40. Tang S, Vickers SM, Hsu HP, Spector M. Fabrication and characterization of porous hyaluronic acid-collagen composite scaffolds. J Biomed Mater Res 2007;82A:323-335.

41. O'Brien FJ, Harley BA, Yannas IV, Gibson L. Influence of freezing rate on pore structure in freeze-dried collagen-GAG scaffolds. Biomaterials 2004;25:1077-1086.

42. Ueda H, Hong L, Yamamoto M, Shigeno K, Inoue M, Toba T, Yoshitani M, Nakamura T, Tabata Y, Shimuzu Y. Use of collagen sponge incorporating transforming growth factor-beta1 to promote bone repair in skull defects in rabbits. Biomaterials 2002;23:1003-1010.

43. Haugh MG. The development of novel scaffolds for tissue engineering with a range of structural and mechanical properties. PhD Thesis, Trinity College Dublin, Ireland, 2008.

44. Hollister SJ, Maddox RD, Tabas JM. Optimal design and fabrication of scaffolds to mimic tissue properties and satisfy biological constraints. Biomaterials 2002;23:4095-4103.

45. Pieper JS, Oosterhol A, Dijkrsta PJ, Veerkamp JH, van Kuppevelt TH. Preparation and characterization of porous crosslinked collagenous matrices containing bioavailable chondroitin sulphate. Biomaterials 1999;20:847-858.

46. Khor E. Methods for the treatment of collagenous tissues for bioprostheses Biomaterials 1997;18:95-105.

47. Pieper JS, Hafmans T, Veerkamp JH, van Kuppevelt TH. Development of tailor-made collagen–glycosaminoglycan matrices: EDC/NHS crosslinking, and ultrastructural aspects. Biomaterials 2000;21:581-593.

48. Wang X, Seed B. A PCR primer bank for quantitative gene expression analysis. Nucleic Acids Res 2003;31(24):e154.

49. Harley BA, Leung JH, Silva ECCM, Gibson LJ. Mechanical characterization of collagen–glycosaminoglycan scaffolds. Acta Biomater 2007;3:463–474.

50. Camacho Nr, West P,Torzilli PA,Mendelson R. FTIR Microscopic Imaging og Collagen and Proteoglican in Bovin Cartilage. Biopolymers (Biospectroscopy) 2001;62,1-8.

51. Wang XH, Li DP, Wang WJ, Feng QL, Cui FZ, Xu YX, Song XH, van der Wert M. Biomaterials 2003;24:3213-3220.

52. Pietrucha K. Changes in denaturation and rheological properties of collagen-hyaluronic acid scaffolds as a result of temperature dependences. Int J Biol Macromol 2005;36:299-304.

53. Tsereteli GI, Belopolskaya TV, Grunina NA. Dehydreted native biopolymers – a unique representative of glassy systems. J Therm Anal Calorim 2008;92:711–716

54. Friess W, Lee G. Basic thermoanalytical studies of insoluble collagen matrices. Biomaterials 1996;17:2289-2294.

55. Engler A, Bacakova L, Newman C, Hategan A, Griffin M, Discher D. Substrate compliance versus ligand density in cell on gel responses. Biophys J 2004;J86:617–28.

56. Wang Y, Yang C, Chen X, Zhao N. Development and characterization of novel biomimetic composite scaffolds based on bioglass-collagen-hyaluronic acid-phosphatidylserine for tissue engineering applications. Macromol Mater Eng 2006;291:254-262.

57. Yannas IV. Tissue and organ regeneration in adults. New York: Springer, 2001.

58. Freyman TM, Yannas IV, Pek Y-S, Yokoo R, Gibson LJ. Micromechanics of fibroblast contraction of a collagen–gag matrix. Exp Cell Res 2001;269:140–53.

59. Gibson LJ, Ashby MF. Cellular solids: structure and properties. 2nd ed. Cambridge, UK: Cambridge University Press, 1997.

60. Gomez-Alejandre S, Sanchez de la Blanca E, Abradelo de Usera C, Rey-Stolle MF, Hernandez-Fuentes I. Partial specific volume of hyaluronic acid in different media and conditions Int J Biol Macromol 2000;27:287–290.

61. Onck PR, Andrews EW, Gibson LJ. Size effects in ductile cellular solids. Part I Modelling. Int J Mech Sci 2001;43:681–99.

62. Andrews EW, Gioux G, Onck P, Gibson LJ. Size effects in ductile cellular solids. Part II: Experimental results. Int J Mech Sci 2001;43:701–13.

63. Wilkison W, Min H, Claffey K, Satterberg B, Spiegelman B. Control of the adipsin gene in adipocyte differentiation. Identification of distinct nuclear factors binding to single-and double-stranded DNA. J Biol Chem 1990;265(1):477.

64. Fajas L, Debril M, Auwerx J. Peroxisome proliferator-activated receptor-gamma: from adipogenesis to carcinogenesis. J Mol Endocrinol 2001;27(1):1.

65. Avram M, Avram A, James W. Subcutaneous fat in normal and diseased states 3. Adipogenesis: from stem cell to fat cell. J Am Acad Dermatol 2007;56(3):472-492.

66. Richon V, Lyle R, McGehee R. Regulation and expression of retinoblastoma proteins p107 and p130 during 3T3-L1 adipocyte differentiation. J Biol Chem 1997;272(15):10117.

67. Ailhaud G, Dani C, Amri E, Djian P, Vannier C, Doglio A, et al. Coupling growth arrest and adipocyte differentiation. Environ Health Persp 1989;80:17.

Captions

Figure 1 μCT images of different cross-sections of freeze-dried scaffolds. (A) pure collagen, transverse view and (B-C) longitudinal views of B-collagen, C-collagen-7.5HA and (d) collagen-15HA. A: area 1- larger pore zone; A: area 2- material densification zone.

Figure 2 SEM micrographs of the longitudinal sections of freeze-dried scaffolds with different content of HA (a)-collagen 100%; (b)-collagen-7.5HA; c)- collagen-15HA. SEM micrographs of the transverse sections of the same scaffolds: (d)-collagen 100%; (e)-collagen-7.5HA; f)- collagen-15HA

Figure 3 XRD patterns of pure collagen and various collagen-HA scaffolds

Figure 4 FTIR spectra of pure collagen and various collagen-HA scaffolds

Figure 5 Example of TG and DSC profile of thermal decomposition of scaffolds

Figure 6 The effect of scaffold composition on the overall water uptake at different soaking time

Figure 7 Swelling percentage corresponding to the scaffold material itself in dependence of its composition and soaking time

Figure 8 SEM micrographs of the longitudinal sections of freeze-dried scaffolds after being swollen in water at 37 ^{o}C 10 days: (a)-collagen 100%; (b)-collagen-7.5HA; c) - collagen-15HA.

Figure 9 Weight loss (%) of different scaffold compositions versus time in distilled water at 37 ^{0} C

Figure 10 Typical profiles of compressive stress–strain curves observed for hydrated collagen and Coll-HA scaffolds:

a) Three repeated testing of the same scaffold specimen in the entire strain range (ε: 0-0.8): **1**- linear elastic zone; **2**- collapse plateau; **3**- densification regime.

b) Strain sub- range ε: 0-0.4 to better show the linear elastic region and the calculation of mechanical properties

Figure 11 Linear elastic (Young's) modulus (**E***) and Collapse plateau modulus **($\Delta\sigma/\Delta\varepsilon$)** □for all hydrated scaffolds

Figure 12 Elastic plateau stress σ^*_{el} (compressive strength) for all hydrated scaffolds

Figure 13 Cell proliferation and adipogenesis of 3T3-L1 preadipocytes within collagen and collagen-mixed HA scaffolds. Cell proliferation (**A)** following 8 days of adipogenic culture expressed as the number of Ki-67 positive cells versus total cell numbers per frame. n=8, * indicates significant elevation versus all other groups by student T-test (p<0.05). Lipid staining by Oil-Red O following 8 days of adipogenic culture within collagen 100% (**B**) and collagen-7.5HA (**C**) scaffolds. S and l indicate regions of scaffold and lipid respectively (bar indicates 100μm). Mean quantitative PCR for Adipsin (**D**) and PPARγ (**E**) mRNA abundance relative to a pooled sample standard and normalized to housekeeping gene cyclophillin A. $n\geq4$ for each sample.

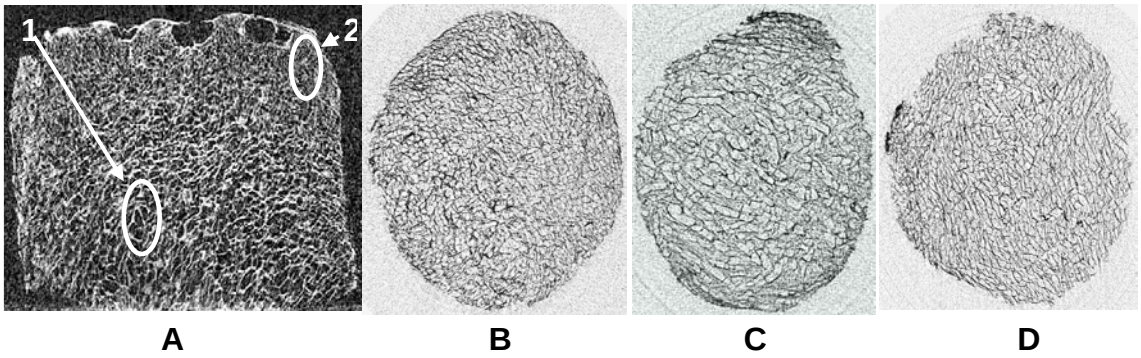

Figure 1

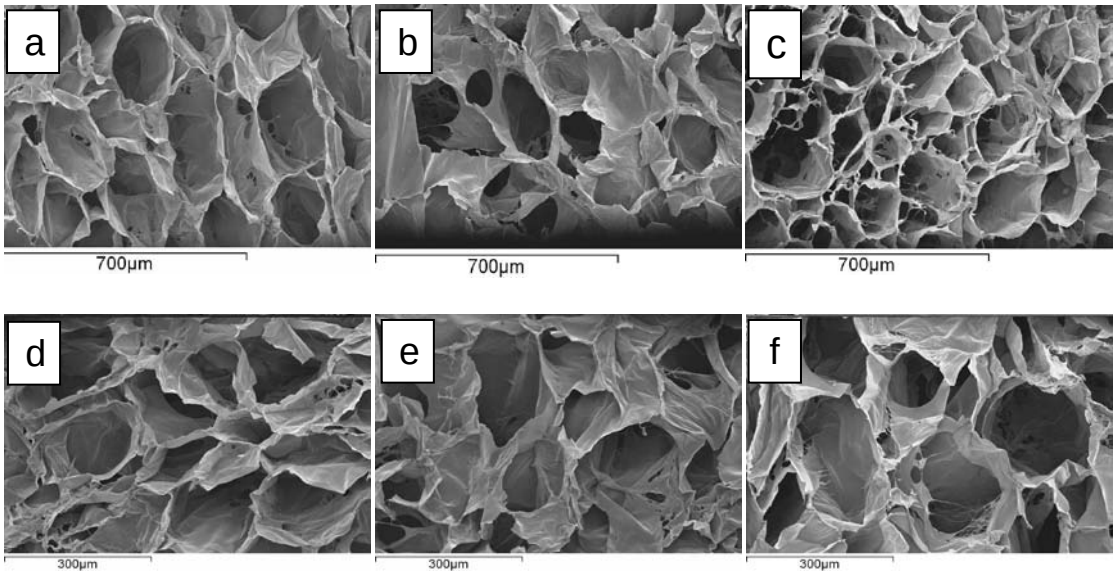

Figure 2

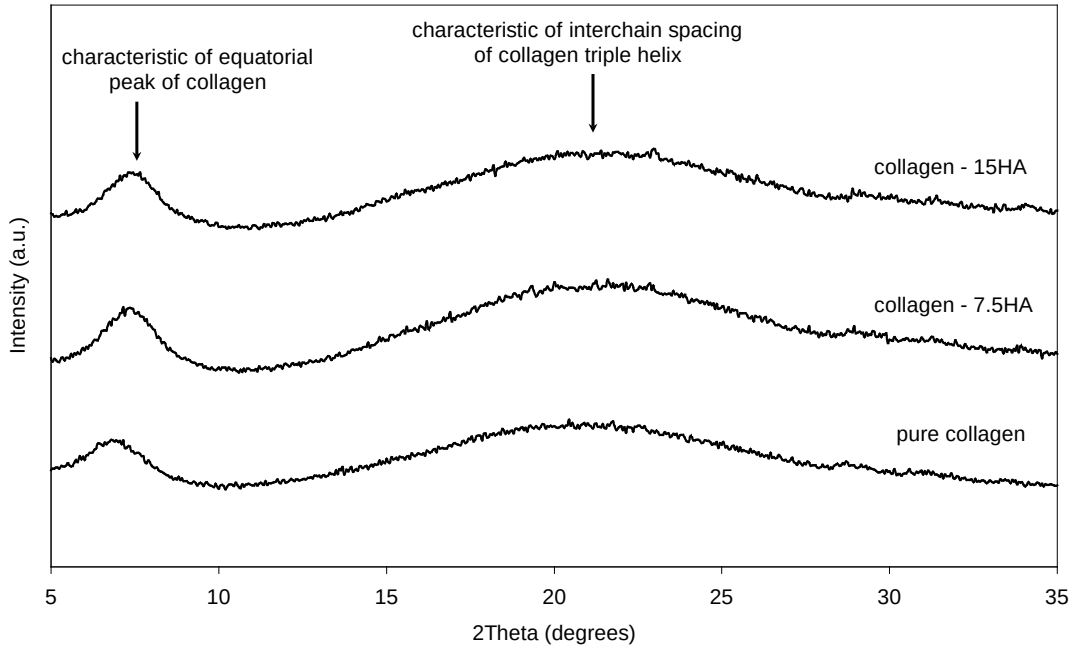

Figure 3

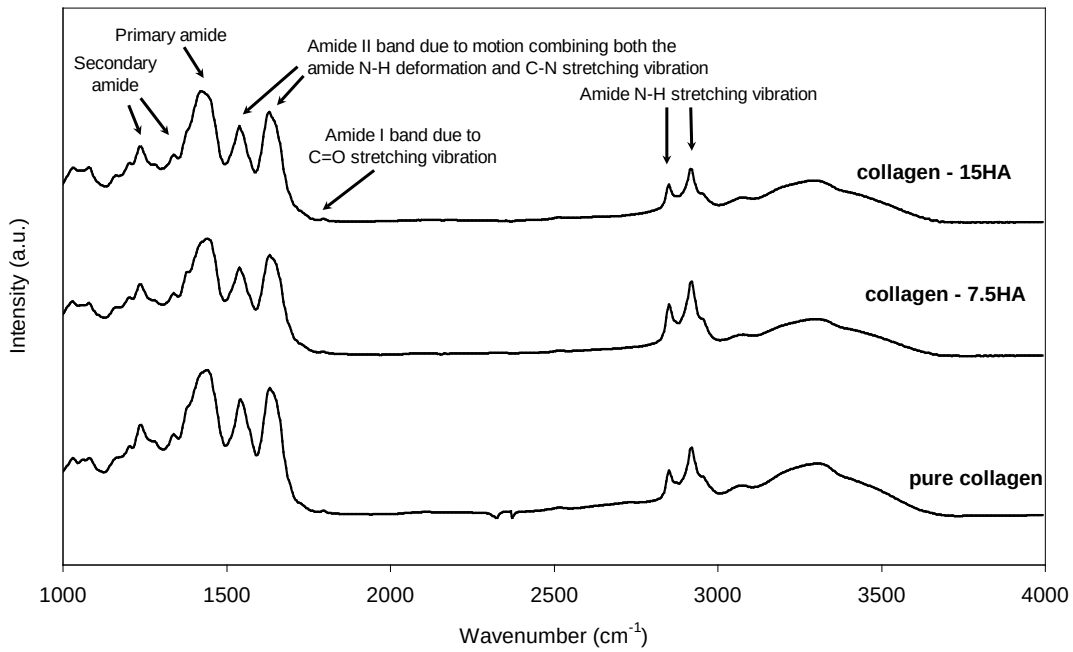

Figure 4

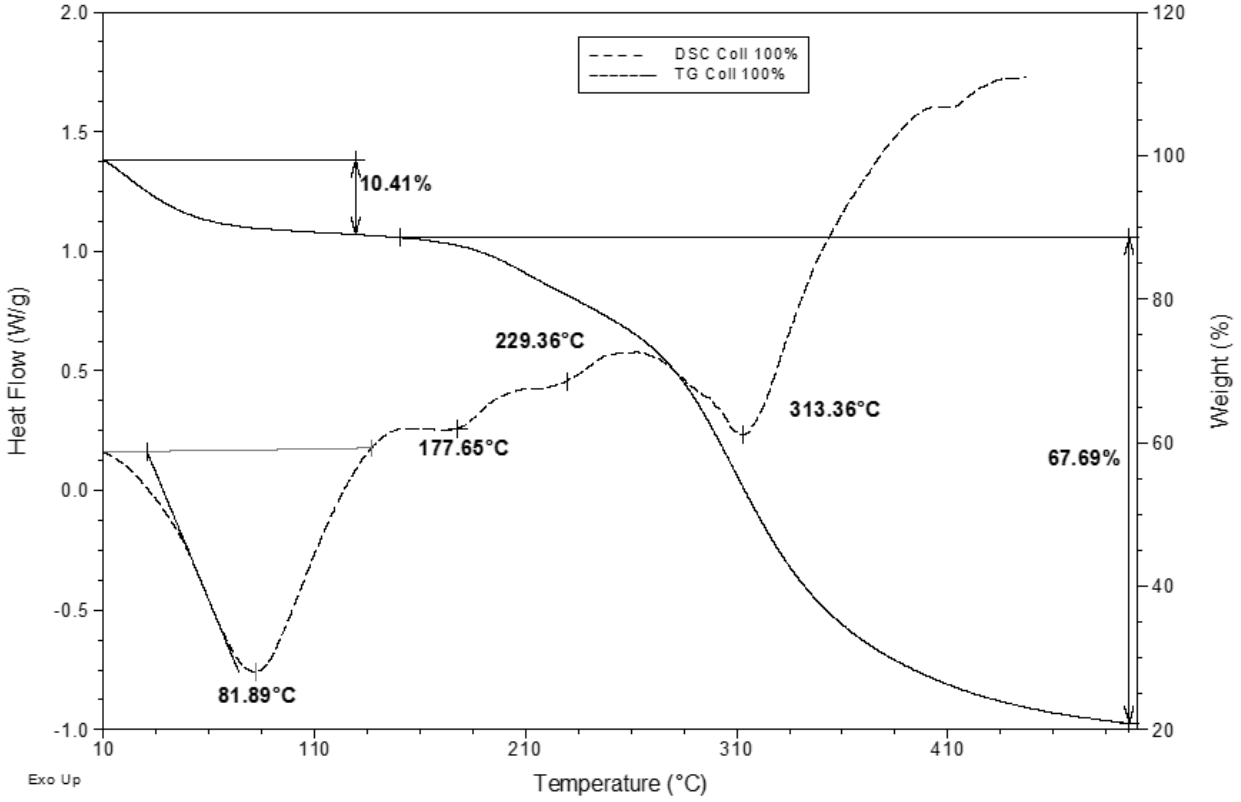
DSC Coll 100%
TG Coll 100%
10.41%
229.36°C
313.36°C
177.65°C
67.69%
81.89°C
Heat Flow (W/g)
Weight (%)
Temperature (°C)
Exo Up
2.0
1.5
1.0
0.5
0.0
-0.5
-1.0
120
100
80
60
40
20
10
110
210
310
410

Figure 5

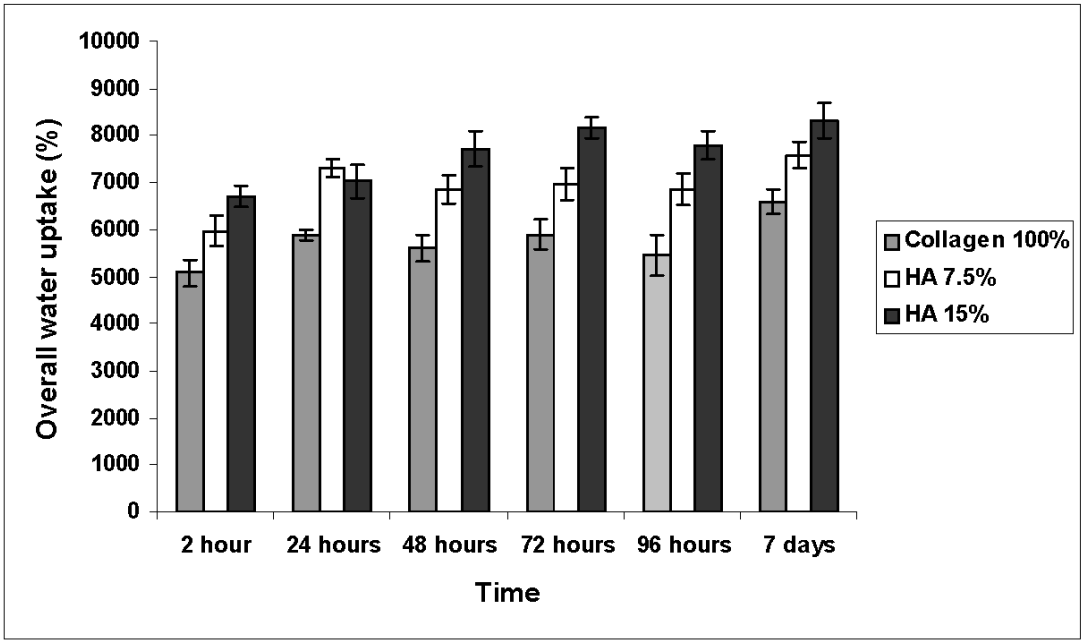
Overall water uptake (%)
10000
9000
8000
7000
6000
5000
4000
3000
2000
1000
0
2 hour
24 hours
48 hours
72 hours
96 hours
7 days
Time
Collagen 100%
HA 7.5%
HA 15%

Figure 6

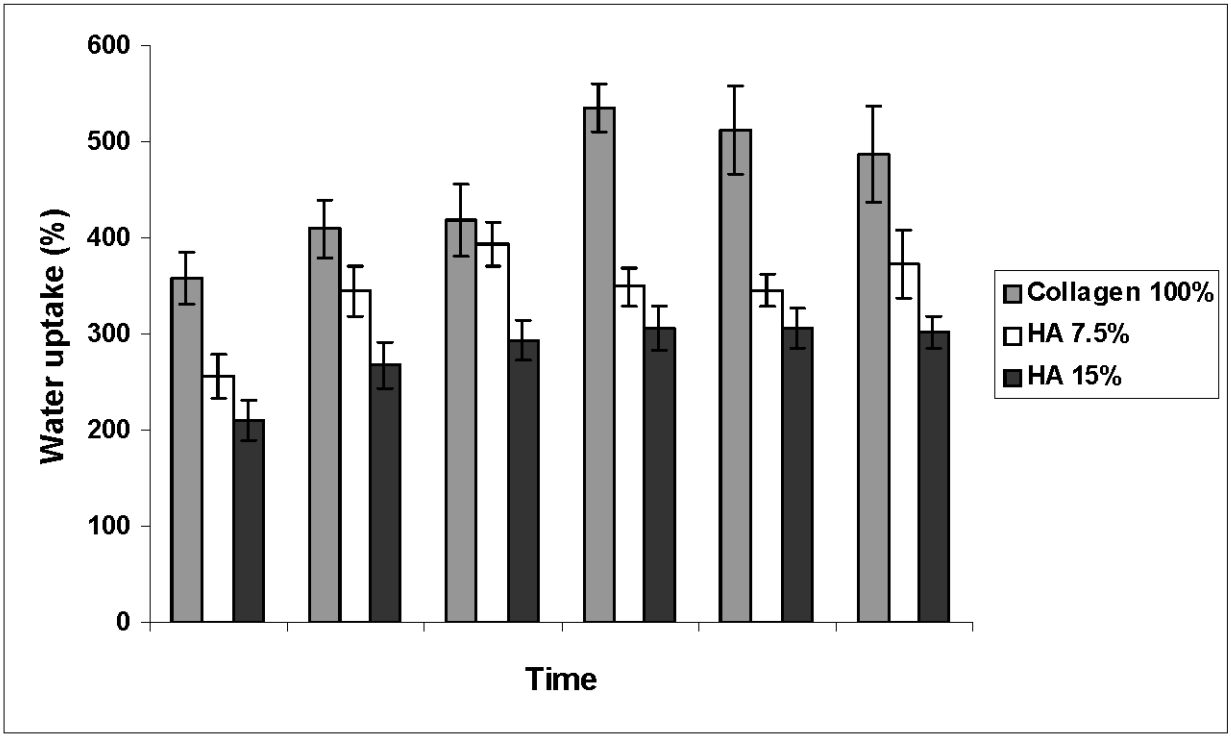
600
500
400
300
200
100
0
Water uptake (%)
Time
Collagen 100%
HA 7.5%
HA 15%

Figure 7

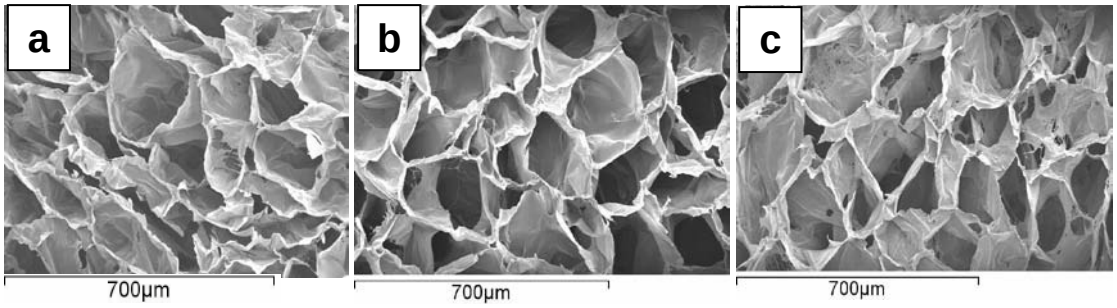

Figure 8

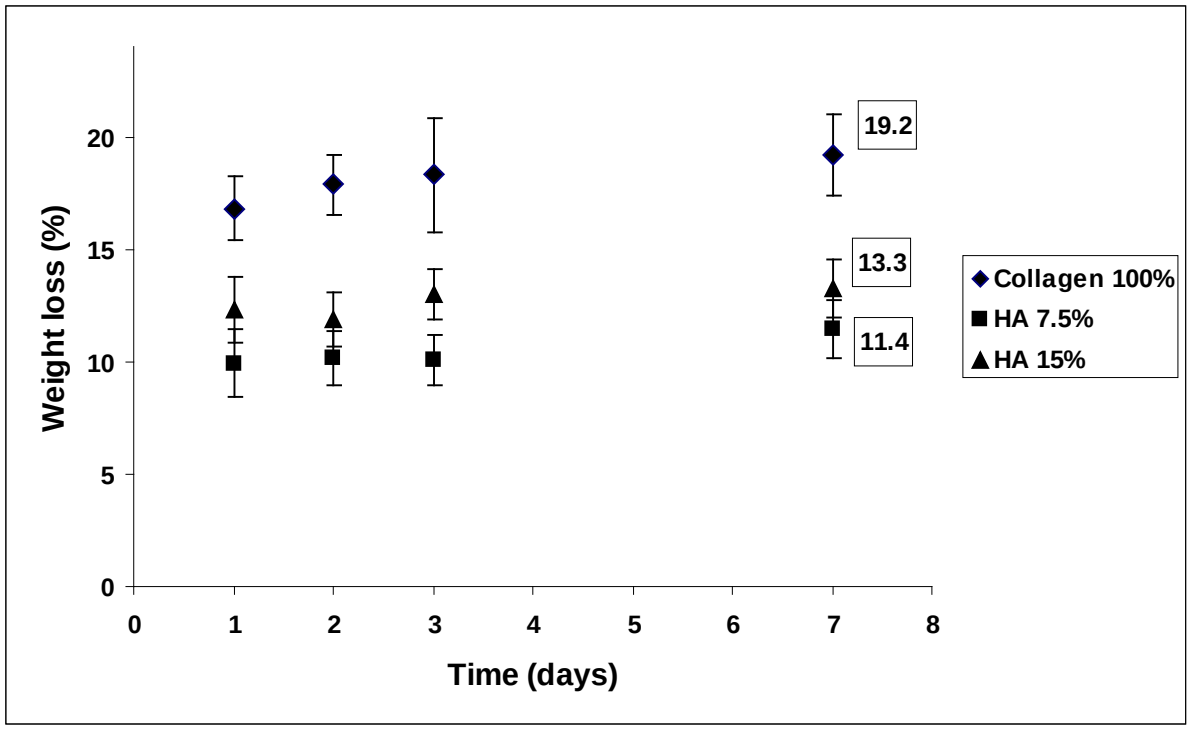

Figure 9

a)

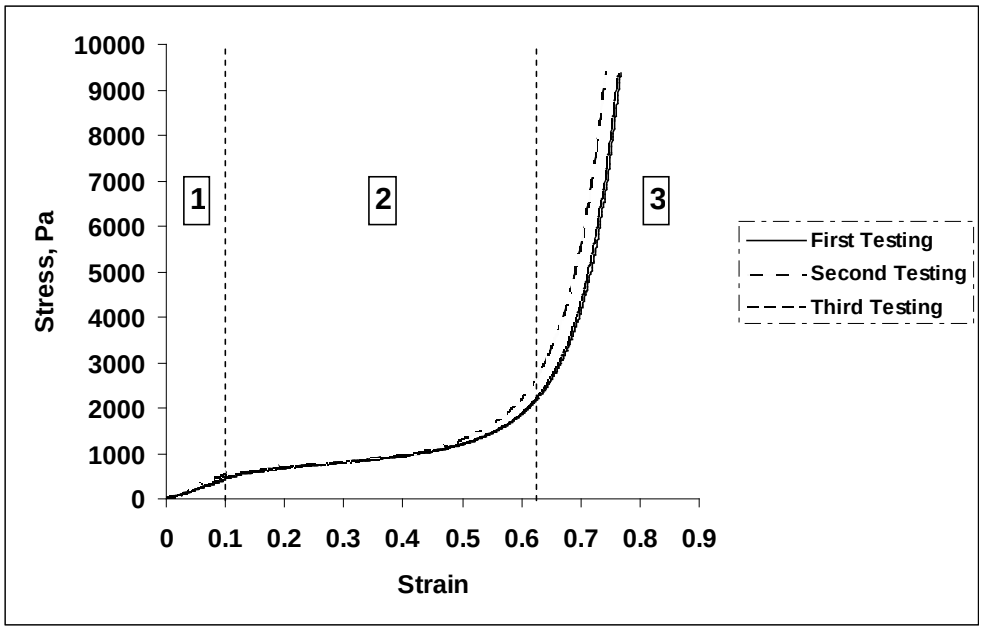
10000
9000
8000
7000
6000
5000
4000
3000
2000
1000
0
Stress, Pa
1
2
3
0
0.1
0.2
0.3
0.4
0.5
0.6
0.7
0.8
0.9
Strain
First Testing
Second Testing
Third Testing

b)

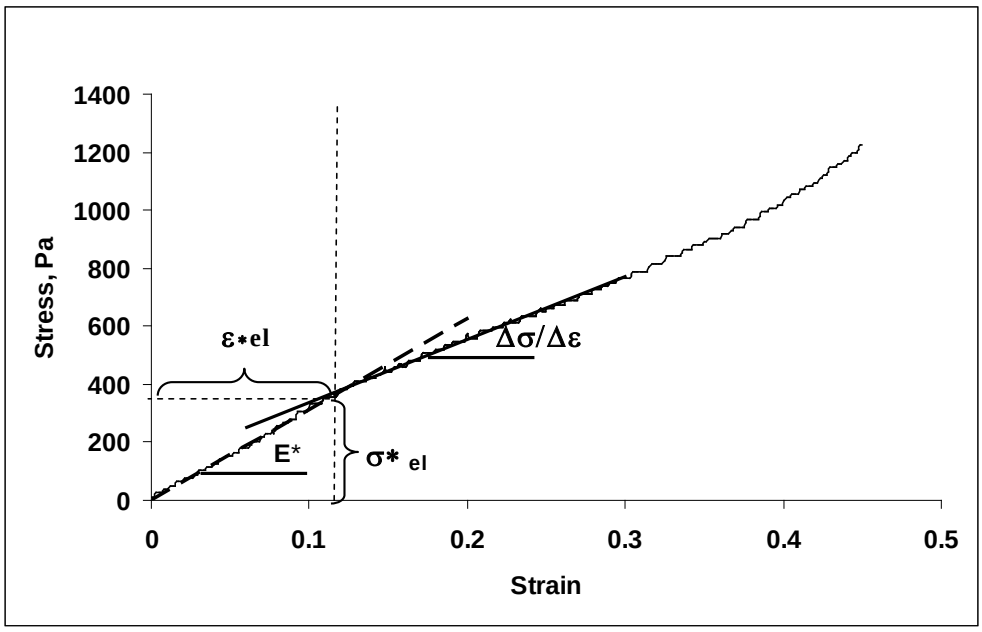
1400
1200
1000
800
600
400
200
0
Stress, Pa
ε*el
Δσ/Δε
E*
σ* el
0
0.1
0.2
0.3
0.4
0.5
Strain

Figure 10

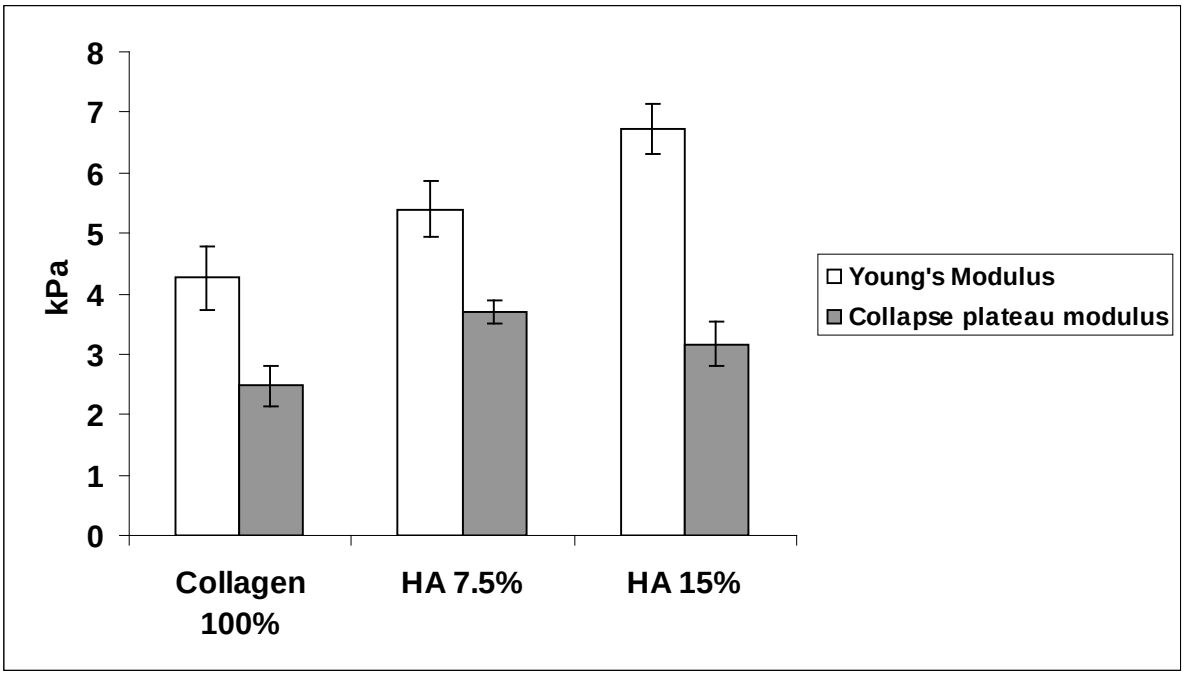

Figure 11

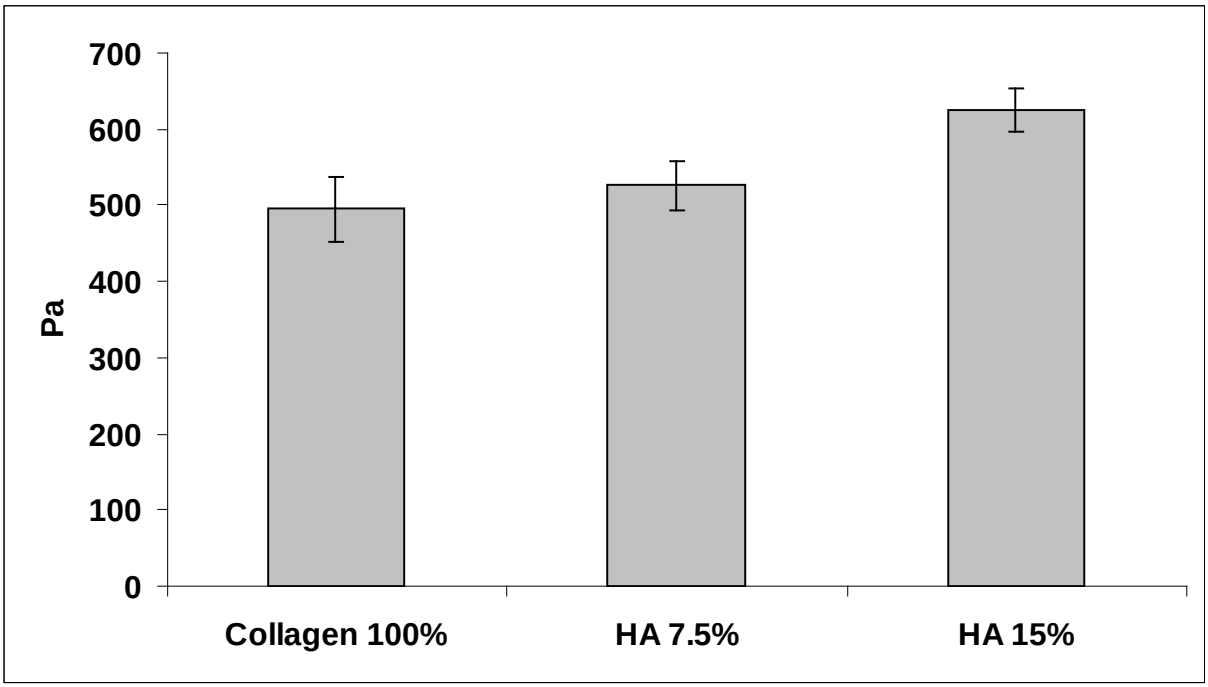

Figure 12

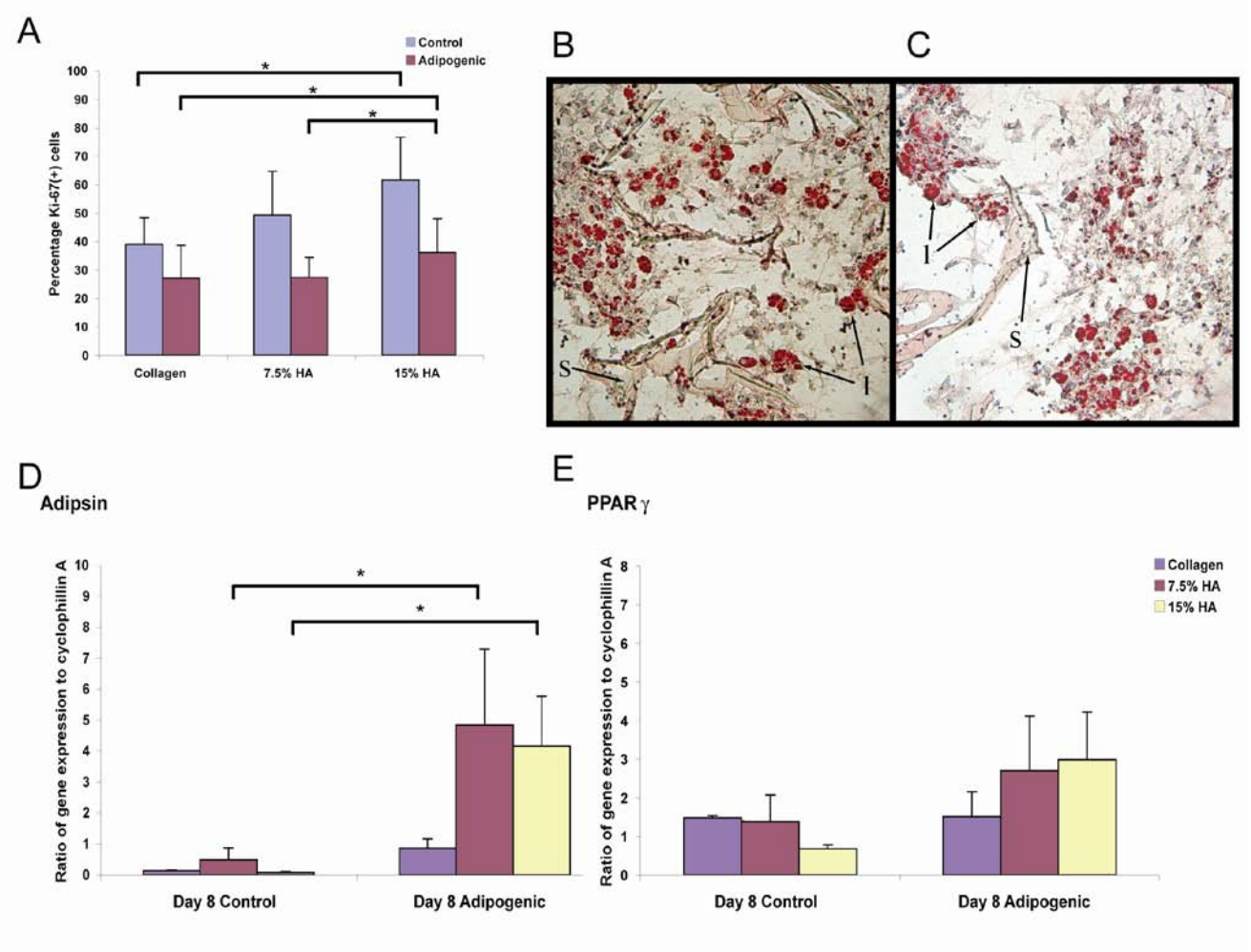
A
Control
Adipogenic
Percentage Ki-67(+) cells
Collagen
7.5% HA
15% HA
B
C
S
I
D
Adipsin
Ratio of gene expression to cyclophillin A
Day 8 Control
Day 8 Adipogenic
E
PPAR γ
Collagen
7.5% HA
15% HA

Figure 13

Table 1 DSC and TG analysis of Scaffolds.

Td: thermal denaturation temperature; T_1-T_3: maximum temperatures for thermal transitions; Δm^1: mass loss at denaturation transition; Δm^2: mass loss at T_1-T_3 transitions; Δm^3: total mass loss at 496 ^{0}C.

Scaffold	Td (^{0}C)	Δm^1 (%)	T_1	T_2	T_3	Δm^2 (%)	Δm^3 (%)
Collagen 100%	79.4± 3.4	10.6	177.5	225.4	310.1	67.1	77.7± 2.0
Collagen -7.5HA	80.2±2.6	11.2	180.4	218.3	306.7	63.2	74.4± 1.5
Collagen -15HA	86.2±1.7	11.3	182.5	219.7	296.0	62.3	73.6± 2.1

Note: Each parameter is the mean of two readings

Table 2 Mechanical properties and relative density of the tested scaffolds

Scaffolds	Relative Density ρ^*/ρ_s	Young's modulus E* (kPa)	Collapse plateau modulus $\Delta\sigma/\Delta\varepsilon$(kPa)	Elastic collapse stress σ^*_{el} (Pa)	Elastic collapse strain ε^*_{el}
Collagen 100%	0.0113±0.0003	4.26±0.53	2.48±0.34	495±43	0.11±0.01
Collagen-7.5HA	0.0124±0.0006	5.39±0.46	3.69±0.19	526±33	0.09±0.01
Collagen-15HA	0.0121±0.0008	6.73±0.41	3.17±0.36	625±29	0.10±0.01

Note: Each parameter is the average value of five separate measurements